Journal of Physics:
Condensed Matter

PURPOSE-LED PUBLISHING™

PAPER • **OPEN ACCESS**

Multiscale modelling of heterogeneous fillers in polymer composites: the case of polyisoprene and carbon black

To cite this article: G Giunta *et al* 2021 *J. Phys.: Condens. Matter* **33** 194003

View the article online for updates and enhancements.

You may also like

- Primitive-path statistics of entangled polymers: mapping multi-chain simulations onto single-chain mean-field models
Rudi J A Steenbakkers, Christos Tzoumanekas, Ying Li et al.
- A molecular dynamics study on the local mobility of cis-polyisoprene within the mixed glassy/rubbery states induced by graphene planes
Thana Sutthibutpong
- Coarse-grained molecular dynamics simulation of cis-1,4-polyisoprene with silica nanoparticles under extreme uniaxial tension
Bin Yuan, Fanlin Zeng, Chao Peng et al.

4-CHANNEL CONFIGURABLE OPEN RF ENGINE FOR QUANTUM EXPERIMENTS

LUGUS

Developed by Instrumentation Technologies

High bandwith arbitraty waveform generator (AWG)
Up to 1.25 GSPS

Open & programmable
Full access to FPGA implementation and firmware

Compatible with control frameworks
LabScript, ARTIQ, etc.

High power outputs
Up to 36 dBm

High-bandwidth feedback control
Open or closed-loop operation, Feedback bandwidth up to 125 MSPS

This content was downloaded from IP address 158.69.200.216 on 17/11/2026 at 20:42

OPEN ACCESS
IOP Publishing
Journal of Physics: Condensed Matter
J. Phys.: Condens. Matter **33** (2021) 194003 (9pp)
https://doi.org/10.1088/1361-648X/abe44e

Multiscale modelling of heterogeneous fillers in polymer composites: the case of polyisoprene and carbon black

G Giunta[1,3,*], M Chiricotto[1], I Jackson[1], H A Karimi-Varzaneh[2] and P Carbone[1,*]

[1] Department of Chemical Engineering and Analytical Science, The University of Manchester, Oxford Road, M13 9PL, Manchester, United Kingdom
[2] Continental Reifen Deutschland GmbH, Jädekamp 30, D-30419 Hannover, Germany

E-mail: g.giunta@uu.nl and paola.carbone@manchester.ac.uk

Received 28 November 2020, revised 27 January 2021
Accepted for publication 8 February 2021
Published 23 April 2021

Abstract

The dispersion of inorganic particles within polymeric materials is an extensively used method to enhance their mechanical properties. One of the major challenges in the simulation of polymer composites is to model the uneven surface of the fillers which strongly affects the dynamics of the adsorbed polymers and consequently the macroscopic mechanical properties of the final composite. Here we propose a new multiscale approach that, using experimental adsorption data, constructs the filler surface to statistically reproduce the surface defects. We use this approach to analyse the structure and dynamics of highly entangled polyisoprene melt in contact with different realistic carbon black samples. We show that the presence of the heterogeneous surface has a negligible influence on the structure of the polymer chains but a major effect on their dynamics and the surface wettability.

Keywords: carbon black, coarse-grain, Kremer–Grest, adsorption isotherm, molecular dynamics, polyisoprene, polymer melt

(Some figures may appear in colour only in the online journal)

1. Introduction

Inorganic fillers, such as carbon black (CB) or silica, are employed as reinforcements in polymers to improve mechanical and rheological properties of high-performance rubber materials [1, 2]. The extent of such reinforcement is determined by the degree of dispersion of the filler particles within the polymer matrix. The dispersion of the filler depends on the polymer-filler affinity which is dominated not only by the chemical composition of polymer and filler but also by the filler's surface defects [3]. CB reinforcements for the rubber industry are produced in a variety of classes and types, depending on the required performance of the final product. This wide range of filler morphology leads to significant variations in the composite performance. For this reason, a fundamental understanding of the relationship between size of particles, surface irregularity, surface activity, filler dispersion and surface area is crucial to facilitate the development of high-performance composites. For example, in automotive applications, it has been demonstrated that tyre rolling resistance, which is the mechanical energy that is converted into heat when tyres move for a unit distance over the road surface, is highly affected by the percentage, dispersion and variation of the CB types employed in tyre manufacturing process [4]. Therefore, over the years, experiments and simulations have been widely employed to better understand the mechanism that influences the mechanical and rheological behaviour of the

* Authors to whom any correspondence should be addressed.
[3] Current address: Soft Condensed Matter, Debye Institute for Nanomaterials Science, Department of Physics, Utrecht University, 3584 CC Utrecht, The Netherlands.

Original content from this work may be used under the terms of the Creative Commons Attribution 4.0 licence. Any further distribution of this work must maintain attribution to the author(s) and the title of the work, journal citation and DOI.

composite at the macroscale by looking at the polymer-filler interface. In particular, molecular simulations have become an invaluable tool to characterise the properties of such interfaces [5–8]. However, the structural and chemical heterogeneity of the filler surface included in the model is often still not representative of the real system [9, 10]. Molecular simulations of polymers at the interface with heterogeneous surfaces have been performed mainly at the coarse-grained (CG) level [11] but the results generally refer to generic polymeric systems. In such context, Raos and Idé [12] have employed molecular simulations of bead-and-spring polymer chains to study the dynamics of a polymer monolayer on a chemically heterogeneous surface consisting of weakly and strong attractive energy sites, by tuning the well depth of the Lennard Jones (LJ) potential. Interestingly, the authors found a non-monotonic dependence of the polymer dynamics on its affinity with the surface when this presents some heterogeneity. In particular, the surface containing 75% of strongly attractive sites and 25% of weakly attractive sites presented the highest diffusion activation energy. This result shows that the behaviour of the polymer chains is influenced by the combination of strong polymer-surface affinity and high spread of interaction sites on the surface (disorder). Similar results have been found by Zheng and co-authors [13] who employed CG simulations to study the dynamics of short polymer chains in contact with curved fillers. By investigating the centre of mass diffusion, the polymers again present a non-monotonic dependence of the diffusion activation energy on the nanoparticle composition. There the authors showed also that the effect of the surface heterogeneity increases when the polymer approaches the glass transition temperature suggesting that the surface heterogeneity might have a more pronounced effect on polymers able to form glassy networks. In a more recent paper, Pastore and co-workers [14] introduced a new CG model consisting of an unentangled polymer melt confined between two walls with a variable degree of heterogeneity. In order to vary the surface heterogeneity, the authors introduced a parameter, α, that varies in a range between -1, indicating an intermixed surface of strong and weak energy sites, and 1 when the sites cluster by forming patchy surfaces of two different interaction energies. The authors showed that the presence of a structured attractive surface slows down the polymer dynamics and that the heterogeneity in the polymer dynamics is enhanced when the wall presents patches with a size comparable with the chain size.

These studies have offered a detailed insight into the role of surface structural and energetic heterogeneities on the dynamics of polymeric systems. Nevertheless, they use a prototype surface model where the position and the nature of the defects do not represent real samples. To fill this gap, here we propose a novel method to generate CG CB surfaces based on experimental data. In the model, the structural defects (cavities and edges) are still imparted by the presence of different energy sites, but in our model, their distribution on the surface and relative attraction energies statistically represent experimental samples such as graphite and amorphous carbon. Furthermore, the CB surface is built so as to reproduce the experimental ratio between the size of the polymer and the patches of clustered defects. Using this model, we investigate the structure and dynamics of entangled polyisoprene (PI) on CB fillers.

2. Model and methodology

2.1. CG model of CB fillers

The CB surface fillers are modelled using a top-down approach. From experimental gas adsorption isotherms of ethene on CB samples [15], it has been shown that the surface of CB fillers presents four different phases: graphite (f_{I}), amorphous carbon (f_{II}), crystallite edges (f_{III}), and cavities (f_{IV}). A schematic representation of the morphology of the different sites ($f_{\mathrm{I–IV}}$) is reported in figure 1.

In the present work we analyse the structure and dynamics of an entangled PI melt in contact with three different CB samples: a pure graphitized sample labelled as N220g and two different partially amorphous samples labelled N115 and CGB (the latter meaning channel-gas-black indicating the experimental method used to obtain it). The percentage of the pure graphite, amorphous carbon and defects for each sample are reported in table 1.

As it is shown in table 1, the graphitized N220g sample presents the maximum degree of crystallinity and phases f_{III} and f_{IV} are only in traces. CGB instead is the sample with the highest percentage of defects (crystalline edges and cavities).

The polymer beads and the substrate interact through the cut and shifted LJ (12–6) potential [16]. The potential parameters (ε, σ and r_{cut}) have been optimised using a bottom-up approach as described in reference [16].

Two main assumptions are made when the graphitic surface is built: (i) the 3D filler can be modelled as a 2D surface due to the fact that the size of the fillers employed in polymer composites is much larger than the average polymer radius of gyration, thus their curvature is large enough to be assumed to be planar, (ii) the surface is modelled as a square lattice, as in our previous work [16] we observed that at this level of coarse-graining the symmetry of the surface does not affect the structural properties of the adsorbed polymer chains.

By knowing the energy parameter (ε) associated with graphite, we can calculate the energy parameters of the other phases, by using the experimental scaling factors reported in table 2. Such scaling factor is calculated as the ratio between the adsorption energy associated to graphite (our reference) and the other phases. Looking at table 2, the adsorption energy of graphite is 16 kJ mol^{-1} and that of amorphous carbon is 20 kJ mol^{-1}, therefore the scaling factor of f_{II} is $\frac{20}{16} = 1.25$. This value is then multiplied by the energy parameter associated with pure graphite [16].

In order to model the CB surfaces that are a realistic and accurate representation of the experimental samples, we devise an algorithm that keeps the fractional distribution of each phase and their relative arrangement close to the experimental ones, reported in table 1. The basic steps of the algorithm are the following: we initially set the total number of graphitic patches (f_{I}) per layer, the distance ($D = 0.245$ nm) [16] between the surface beads and the fractions of each phase based on the experimental distribution of table 1. The patches,

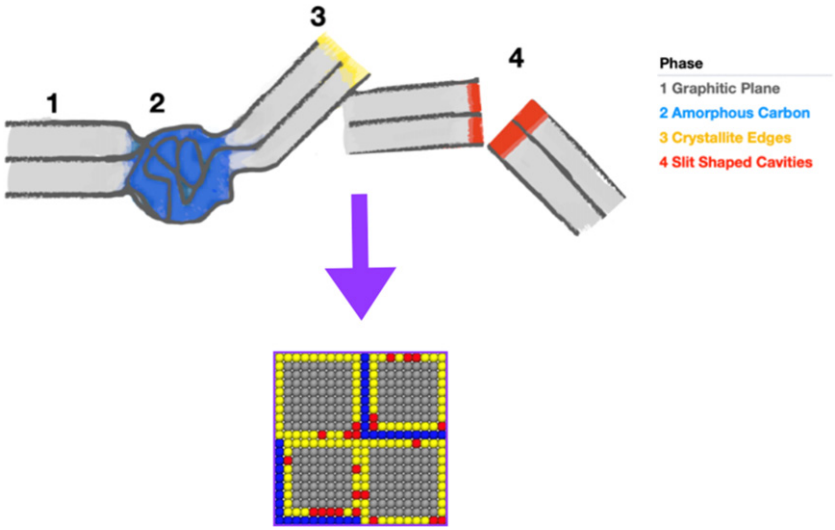


Figure 1. Generation of the 2D model from the CB samples. On the top we report a pictorial representation of a CB filler surface, that is translated in a 2D surface (on the bottom) according to our model. Grey, blue, yellow, and red beads represent in order: graphitic sites (f_{I}), amorphous carbons sites (f_{II}), crystallite edge sites (f_{III}) and slit shaped cavity sites (f_{IV}). This colour code is used for all the figures reported in the remain part of the text.

Table 1. Experimental (Exp.) and calculated (Sim.) percentage of the different phases (f) of the CB samples studied. The experimental values reported are taken from reference [3].

CB Surface		f_{I}	f_{II}	f_{III}	f_{IV}
Graphitized N220g	Exp.	99	0	<1	<1
	Sim.	100.0	0	0	0
N115	Exp.	69	13	15	3
	Sim.	66.0	16.0	14.8	3.2
Channel-gas-black	Exp.	61	2	31	6
	Sim.	58.6	6.8	29.2	5.4

Table 2. Experimental adsorption energies taken from reference [15] of ethene on the different CB phases.

Phase	Adsorption Energy (kJ mol^{-1})	Scaling factor
I	16	1
II	20	1.25
III	25	1.5625
IV	30	1.875

which are initially considered to be square, are then placed on a square lattice of amorphous carbon (f_{II}), that we call entrapment. We determine the average patch size ($p \times D$) by using equation (1), where p is the number of surface beads along the edge of the patch.

$$f_{\mathrm{I}}\,(4p-4) = (f_{\mathrm{III}} + f_{\mathrm{IV}})(p-2)^2. \tag{1}$$

Equation (1) ensures that the defects (edges, f_{III}, and cavities, f_{IV}) are placed only on the boundaries of the graphitic patches.

The average entrapment size, e, defined as the number of beads of purely amorphous phase f_{II} between the patches, is computed by using equation (2).

$$e^2\,(1 - f_{\mathrm{II}}) = p^2. \tag{2}$$

In this way we ensure that the entrapment is composed only of amorphous carbon.

Once the sites for the entrapment and graphitic phase are allocated, we then distribute the two different types of structural defects (edges, f_{III} and cavities, f_{IV}) replacing the edges of the graphitic patches with either type of defects depending on their fractions (table 1). Since we can have crystalline edges and cavities only when two crystalline structures are in contact, we impose that the areas of the surface representing the amorphous phase (f_{II}) cannot contain single isolated defect (i.e. f_{III} or f_{IV} single site).

In figure 2 we report three snapshots of the three CB surfaces, obtained according to our approach.

In order to investigate the effect of the patch size, for the N115 sample, we rescale the patch size p and the entrapment size e. For small patch size, the fraction f_{III} or f_{IV} will increase because we are mapping the 2D space with smaller patches, therefore the number of points on the edges of the patch will increase. In order to restore the original fraction of each phase, we randomly replace beads of f_{III} or f_{IV} with graphitic ones until we reach values close to the experimental fractions. In this way we will obtain jagged patches keeping the initial rules we imposed, i.e. amorphous carbon (f_{II}) cannot contain f_{III} and f_{IV}. In figure 3 we show the snapshots of the CB model surfaces representing the N115 sample with different patch sizes, i.e. 2.2 nm ($\mathrm{N115_b}$), and 1.4 nm ($\mathrm{N115_s}$), obtained by rescaling the initial values of p and e of 1/2 and 1/3. Such patch sizes are selected to maintain the ratio between the polymer radius of gyration ($R_{\mathrm{g}} = 4.36 \pm 0.15$ nm in our simulations) and the average patch size, close to the experimental value, ranging from ∼2 to ∼10 [17, 18].

2.2. CG model of PI melt

The PI melt is described using the modified version of the Kremer–Grest model of Svaneborg *et al.* [19, 20] In such model,

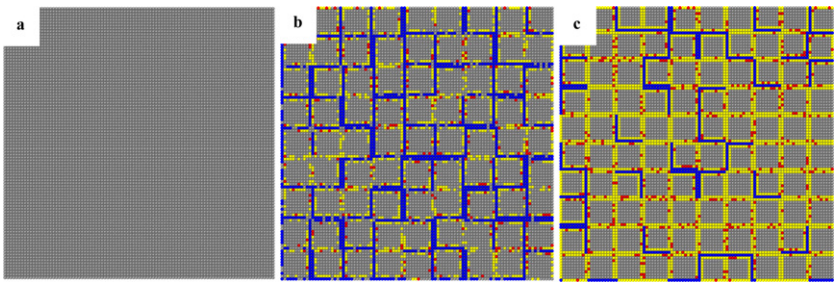


Figure 2. Snapshots of three different CB surfaces. (a) N220g; (b) N115; and (c) CGB. Grey, blue, yellow, and red beads represent in order graphitic planes (f_{I}), amorphous carbons (f_{II}), crystallite edges (f_{III}), slit shaped cavities (f_{IV}).

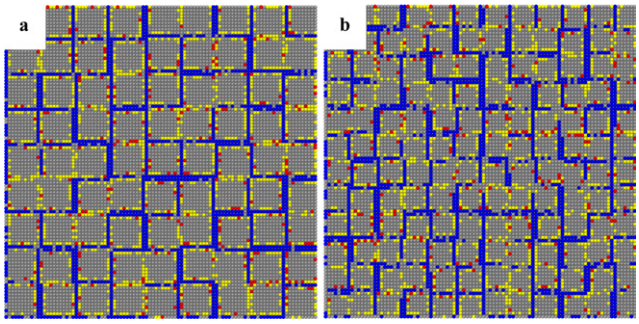


Figure 3. Snapshots of two N115 CB samples of different patch size (a) 2.2 nm and (b) 1.4 nm.

the CG sites, representing roughly one monomer of PI melt, are lumped together into spherical beads. Interactions between CG beads are described with the WCA pair potential:

$$U_{\mathrm{WCA}}(r) = 4\varepsilon\left[\left(\frac{\sigma}{r}\right)^{12} - \left(\frac{\sigma}{r}\right)^{6} + \frac{1}{4}\right] \quad \text{for } r < 2^{1/6}\sigma, \quad (3)$$

where $\varepsilon = k_{\mathrm{b}}T$ is the potential well depth and σ is the separation distance when the potential is zero. Bonded interactions between the beads are described trough the sum of the WCA (equation (3)) and the FENE potential:

$$U_{\mathrm{FENE}}(r) = -\frac{kR^2}{2}\ln\left[1 - \left(\frac{r}{R}\right)^2\right], \quad (4)$$

where $R = 1.5\sigma$ is the maximum allowed distance between the bonded beads and $k = 30\varepsilon\sigma^{-2}$ is the constant force. The minimum of the sum of the two functions sets the equilibrium bond length equal to 0.965σ at a reduced temperature of $T^* = 1$ ($T^* = Tk_{\mathrm{B}}\varepsilon^{-1}$) with k_{B} being the Boltzmann constant at a reduced density of $\rho_{\mathrm{b}} = 0.85\sigma^{-3}$. To restrict chain conformations an additional angle bending interaction is used:

$$U_{\mathrm{bend}}(\theta) = \kappa(1 - \cos\theta), \quad (5)$$

where θ is the angle between successive bonds and κ is the stiffness parameter. A more detailed description of the polymer model can be found in references [16, 20, 21].

2.3. Simulation details

The simulation box (figure 4) is an orthorhombic cell, the sizes of the boxes are reported in table 3. The surface, located at $z = 0$, is composed of 6 identical layers and extends for 1.675 nm along z direction with an interlayer spacing of $\Delta z = 0.335$ nm. Periodic boundary conditions are applied in all directions, therefore the polymer results confined between two solid walls.

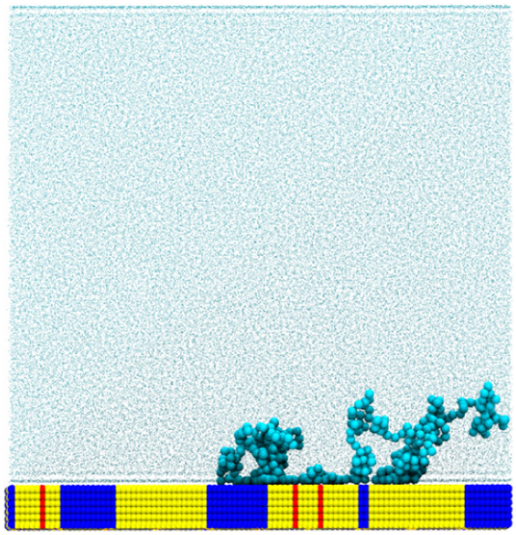


Figure 4. Snapshot of the equilibrated system consisting of PI (cyan) in contact with the CGB filler. For clarity we represent only one polymer chain, the other polymer beads are represented as points. For the colours of the filler surface refer to figure 1.

Table 3. Computational details of the systems simulated in this work.

System	Average Patch size (nm)	$Lx = Ly$ (nm)	Lz (nm)
PI bulk	—	24.25	23.55
PI-N220g	—	24.25	25.60
PI-N115$_{\mathrm{b}}$	2.2	24.01	26.10
PI-N115$_{\mathrm{s}}$	1.4	23.27	27.64
PI-CGB	2.0	24.25	25.60

Molecular overlaps of chain segments in the initial configurations are removed by energy minimisation. During the equilibration period (of duration of 100 ns) the polymer-surface interactions are switched off to allow a quick equilibration of the polymer melt. In the production runs the systems are simulated for up to 2 μs. In the simulations the number of particles, the volume and temperature are kept constant (NVT ensemble). The volume is selected to obtain the experimental

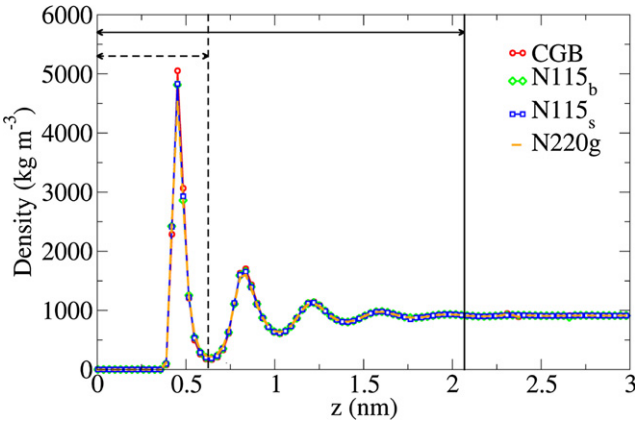


Figure 5. Polymer density profile along the z direction. The different curves refer to the PI in contact with different CB samples: N220g (orange dashed line); N115$_s$ (blue squares); N115$_b$ (green diamonds) and CGB (red circles). The black dashed line defines the adsorbed region (0.625 nm from the outer layer of the solid substrate), while the solid black line defines the interfacial layer (2.068 nm from the outer layer of the solid substrate).

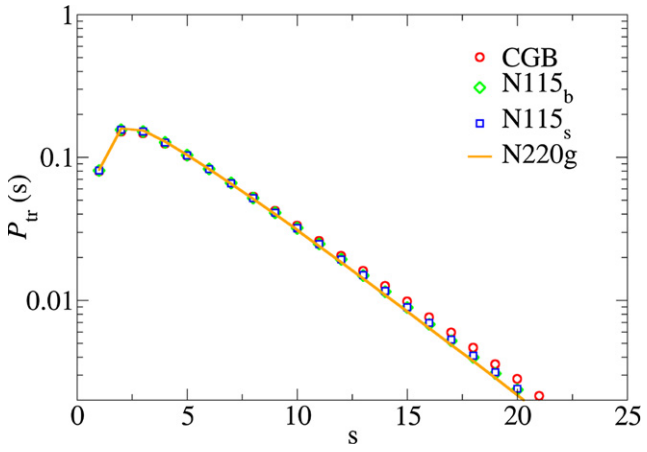


Figure 6. Probability distribution of trains of length *s*. The different curves refer to the PI in contact with different CB samples: N220g (orange solid line); N115$_s$ (blue squares); N115$_b$ (green diamonds) and CGB (red circles).

density of the polymer (910 kg m^{-3}) [21]. The PI melt contains 416 polymer chains consisting of 400 beads. As shown in our previous paper [16], this chain length is long enough to have entanglements in the bulk. This is in agreement with data reported in references [20, 22] where the characteristic number of Kuhn segments between entanglements for PI is reported to be 24.15. The system evolves according to Langevin dynamics [23]. The equations of motion are integrated with a time step of 0.01τ, where $\tau = \sigma\ (m_b\varepsilon^{-1})^{0.5}$ with m_b being the mass of the bead. The friction coefficient is set at $\Gamma = 0.5 m_b \tau^{-1}$. During the simulations, pair interactions between surface beads are neglected and the surface beads are frozen in all directions. All the simulations are carried out using the software GROMACS 2016 [24].

3. Results

We start by investigating the structure of the polymer melt in contact with the four different CB samples. To evaluate the magnitude of the influence of the different substrates, due to the presence of defects of higher energy, we analyse the polymer local density profile (figure 5). The density profile presents an oscillatory behaviour in the vicinity of the surface with three evident peaks. Interestingly, the presence of heterogeneous surfaces with stronger energy sites compared to the N220g sample has a negligible effect on the local density.

Such observations are confirmed by looking at the probability distribution of trains (figure 6). A train of length *s* is defined as the number of bonds connecting two successive beads that reside within a distance, *d*, from the surface equal to 0.625 nm. The distance *d* is defined as the distance from the surface where the first minimum in the density profile (figure 5) occurs. In all the systems the probability distribution of trains presents an exponential decay with high probability of short trains, as predicted from theoretical and other computational works

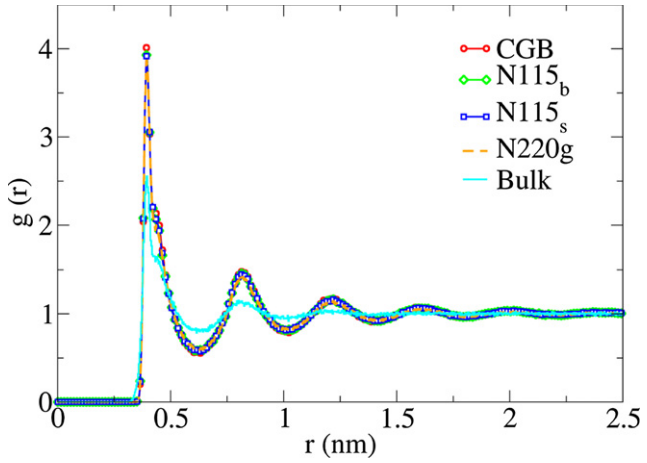


Figure 7. 2D radial distribution function ($g(r)$) between the polymer beads calculated in the *xy* plane in the adsorbed region and in the bulk. The different curves refer to the PI bulk (cyan solid line) and PI in contact with different CB samples: N220g (orange dashed line); N115$_s$ (blue squares); N115$_b$ (green diamonds) and CGB (red circles).

performed with graphite, corresponding to the sample N220g in this work [5, 7, 25].

The mild effect of the surface heterogeneity on the polymer structure is in part due to the fact that the sites with the strongest interactions (the slit shaped cavities, f_{IV}), are less in number compared to the graphite sites and the ratio between the energy parameters for the different phases is small (table 2).

Since we are interested in studying the local structural changes in the plane tangential to the surface, as these depend on the morphology of the substrate, we calculate the 2D radial distribution function ($g(r)$) in the (xy) plane parallel to the surface as a function of the distance from the solid substrate. In figure 7 we report the 2D $g(r)$ between the polymer beads for the different systems, calculated in a slab of width corresponding to half of the bead size in the adsorbed region (see definition in figure 5). Using the same strategy, we also

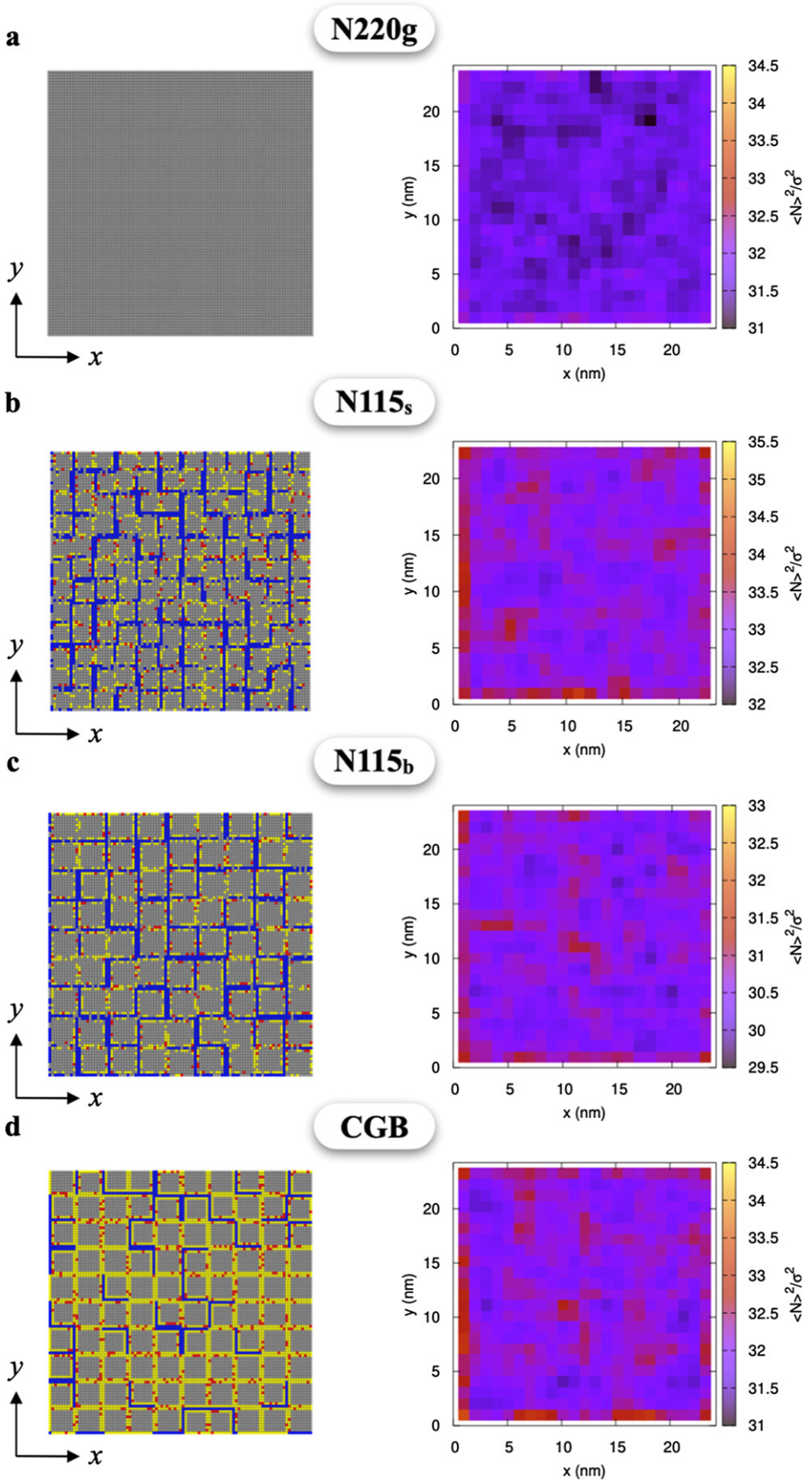


Figure 8. Inverse normalised fluctuations (on the right) and corresponding surface morphologies (on the left) for the polymer in contact with (a) N220g; (b) $N115_s$; (c) $N115_b$ and (d) CGB, calculated over 20 000 configurations.

calculate the 2D $g(r)$ in the middle of the simulation box where the polymer bulk density is recovered (figure 7 cyan line).

From figure 7 we can observe that the polymer chains in contact with the solid substrate are more packed than those in the bulk region. Again, we observe that the presence of defects on the surface has a negligible effect on the polymer chain conformation.

To understand the effect of the heterogeneity of the substrate we calculate the inverse normalised fluctuation [26]:

$$\frac{\langle N\rangle^2}{\sigma^2}, \tag{6}$$

where $\langle N\rangle$ is the average number density and σ is the average number density fluctuation calculated as the standard deviation of the density. In order to perform such calculations, we divide the box in cells of height, in z direction, corresponding to the value of the adsorbed region (0.625 nm, first minimum in the density profile, figure 5) and of $\sim$1 nm, in order to be smaller than the minimum length of the patches, in x and y directions.

In figure 8 we report the inverse normalised fluctuations calculated only in the layer adjacent to the surface for the four different fillers.

Figure 8 shows that the inverse normalised fluctuation provides a sensitive measurement to detect the effect of the surface roughness. The fluctuation is relatively flat when the polymer is in contact with N220g, but it presents peaks when the polymer is in contact with the fillers with surface defects. The height of the $\frac{\langle N\rangle^2}{\sigma^2}$ peak at a given location on the surface is related to its wettability: high peaks indicate lower density fluctuation and thus better surface wetting, while lower peaks indicate less adhesion between the polymer and the filler [26]. Therefore figure 8 shows that fillers with surface defects should be easier to disperse in the polymer matrix than type N220g.

To study the effect of heterogeneous fillers on the dynamics of the polymer chains, we calculate the autocorrelation function of the end-to-end vector $\boldsymbol{R}_{\rm ee}$:

$$C(t) = \frac{\langle P_2[\boldsymbol{R}_{\rm ee}(0)\cdot\boldsymbol{R}_{\rm ee}(t)]\rangle}{\langle \boldsymbol{R}_{\rm ee}(0)^2\rangle}, \tag{7}$$

where P_2 is the second order Legendre polynomial, $\left(\text{i.e.}, P_2(x) = \frac{1}{2}(3x^2-1)\right)$ [27].

The corresponding relaxation time $\tau_{\rm R}$, is calculated by fitting the autocorrelation function (figure 9) to a stretched exponential function (equation (8)), also called Kohlrausch–Williams–Watts (KWW) function [28–30]:

$$C(t) \approx \exp\left[-\left(\frac{t}{\tau_{\rm KWW}}\right)^{\beta}\right], \tag{8}$$

where β is the stretching parameter. The values of $\tau_{\rm R}$ are obtained as follows:

$$\tau_{\rm R} = \frac{\tau_{\rm KWW}}{\beta}\Gamma\left(\frac{1}{\beta}\right), \tag{9}$$

where $\Gamma\left(\frac{1}{\beta}\right)$ is the gamma function of $1/\beta$. The fitting is performed until $C(t) = \frac{1}{e}$.

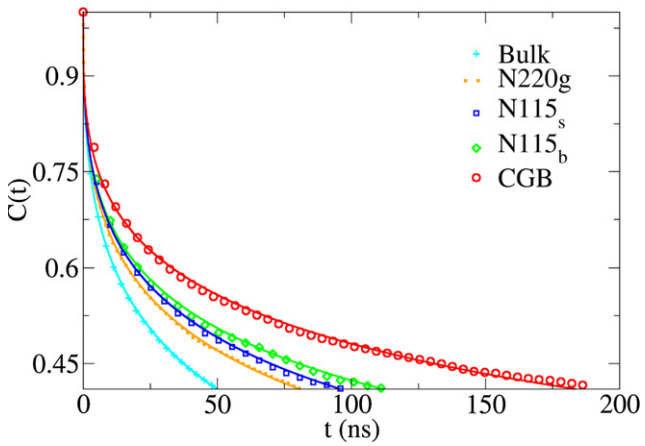


Figure 9. Autocorrelation function of the end-to-end vector (symbols) and the corresponding fitting (solid lines). The different curves refer to the PI bulk (cyan plus) and in contact with different CB samples: N220g (orange dots); $N115_s$ (blue squares); $N115_b$ (green diamonds) and CGB (red circles).

In figure 9 we report the autocorrelation functions of the end-to-end vectors of the polymer chains having their centre of mass (COM) within the interfacial layer of width 2.068 nm (5σ) [7, 16], (see definition in figure 5). Since the system is confined between two walls, we average the values of the autocorrelation functions in the two slabs adjacent to the substrate.

From figure 9 we notice that polymers in contact with surfaces with increasing surface defects present the slowest dynamics. These changes in local dynamics can be related to changes in the polymer glass transition temperature, as the slower the autocorrelation decays the higher the glass transition temperature of the polymer is [31]. Interestingly, the polymer chains in contact with fillers presenting same percentage of phases (N115) but different graphitic patch size, show a different behaviour. The chains in contact with $N115_s$ (small patches) are characterised by a faster relaxation compared to the chains in contact with $N115_b$ (big patches). This indicates that for same filler heterogeneity, big patches have more influence on the relaxation of the polymer chains. This might look counterintuitive as one might think that a polymer chain interacting with a surface with large graphitic patches should have a dynamic behaviour similar to that when in contact with N220g. However, the result seems to indicate that surfaces with small patches are seen by the polymer as homogeneous surface with averaged surface properties. Pastore and co-authors [14] have also found that the heterogeneity in the polymer dynamics is enhanced when the solid substrate presents patches with a size at least comparable with the polymer chain size. The value of β, reported in figure 11, is also indicative of dynamic heterogeneity with lower values of β characteristic of systems with wider distribution of relaxation times, larger deviations from the Debye behaviour and higher degree of heterogeneity [30, 32]. Here the value of β consistently changes across the various samples: in bulk the value is the highest and it reduces when the filler is introduced. The inclusion of surface defects reduces further the value of β with the lowest value reached for the CGB sample.

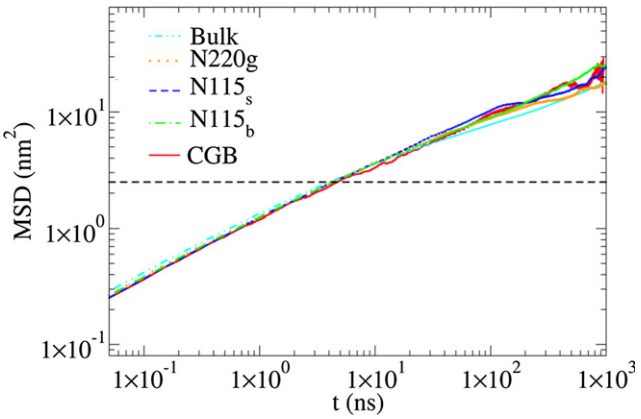


Figure 10. Mean-square-displacement of the polymer central-bead. The different curves refer to the PI bulk (cyan – · ·–) and in contact with different CB samples: N220g (orange · · ·); $N115_s$ (blue ––); $N115_b$ (green – · –) and CGB (red –).

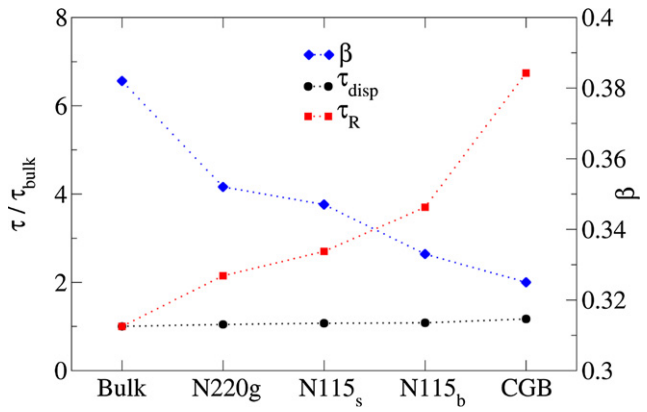


Figure 11. Dynamic decoupling: stretching parameter, β (blue diamonds); normalised displacement time (black circles) and relaxation time (red squares). The dotted lines are guide for the eye.

A common measure of the translation dynamics of polymer chains in a planar confinement is their central-bead mean-square-displacement (MSD) calculated in the plane parallel to the surface (xy) [33, 34]:

$$\mathrm{MSD}_{\parallel} = \langle (x(t) - x(t_0))^2 + (y(t) - y(t_0))^2 \rangle. \qquad (10)$$

Due to the high molecular weight of the polymer melt, the free diffusion of the chain central bead could not be reached within the simulation time. We then calculate the MSD of the central monomers of the polymer chains in bulk at an arbitrary time of 4 ns, which corresponds to a $\mathrm{MSD}_{\parallel} = 2.5\ \mathrm{nm}^2$, and compare this time with the times required by the chains in contact with the different fillers to reach the same displacement. We refer to this time as displacement time, $\tau_{\mathrm{disp.}}$

To calculate the MSD of the polymer chains in contact with the substrates we track the z coordinates of the COM of the polymer chains during the simulation time and then calculate the polymer central-bead MSD of the chains whose COM in average do not leave the interfacial layer. In figure 10 we report the MSD of the different systems.

In agreement with the results by Rissanou and Harmandaris [30], we find that overall the global chain dynamics is only mildly affected by the presence of the substrate, as it is shown in figure 10 and by the values of τ_{disp} in figure 11. In figure 11 we also plot along with the values of τ_{disp}, τ_{R} (both normalised by the corresponding times calculated in bulk τ_{bulk}) and β. The inclusion of the graphitic surface into the polymer melt leads to a decoupling between the chain diffusion, τ_{disp}, and its relaxation time, τ_{R}: the former maintains the same value and the latter increases (figure 11). As observed by Pastore and co-workers for a generic CG model [14], the decoupling becomes even more pronounced for surfaces with defects where τ_{R} increases with the amount of surface defects while τ_{disp} remains almost constant. The maximum decoupling is observed for the filler with the highest number of high energy defects, CGB, for which β reaches its lowest value. Such decoupling, due to the presence of fast and slow particles, indicates again dynamic heterogeneity in the sample.

4. Conclusions

We have proposed a method to build realistic CB fillers morphologies and we have employed it to study the structural and dynamic behaviour of an entangled melt of PI. From the structural analysis we observed that the presence of a heterogeneous surface does not have a strong influence on the local structure of the polymer chain, but has a sizeable effect on the surface wettability and therefore most likely the fillers dispersion. The dynamics of the polymer chain at the interface is also strongly influenced. In this case however not only the nature of the defects is important but also their relative distribution and the sizes of the crystalline phase. We found a noticeable dynamic heterogeneity due to the presence of the solid surface and observe that this heterogeneity becomes more evident for the surfaces containing defects and reaches its maximum for the surface representing the filler with the highest concentration of high energy defects (crystalline edges). Our approach to build filler surfaces statistically representative of the experimental samples is therefore able to discriminate between different CB experimental samples and can help in identifying structure-properties relationships in polymer composites. The procedure can also be applied to any other inorganic particles for which adsorption data are available.

Acknowledgments

Computational facilities for this work were provided by the Computational Shared Facility (CSF) of the University of Manchester. The authors thank Dr Frank Fleck for the useful discussions. GG thanks the EPSRC funded Centre for Doctoral Training ‘Materials for Demanding Environments’ EP/L01680X/1 and Continental Tires for the financial support. MC, AK and PC thank the European Union’s Horizon 2020 research and innovation programme project VIMMP under Grant Agreement No. 760907.

Data availability statement

All data that support the findings of this study are included within the article (and any supplementary files).

ORCID iDs

G Giunta https://orcid.org/0000-0002-8986-9604
M Chiricotto https://orcid.org/0000-0003-1609-5254
H A Karimi-Varzaneh https://orcid.org/0000-0002-7661-3490
P Carbone https://orcid.org/0000-0001-9927-8376

References

[1] Möwes M M, Fleck F and Klüppel M 2014 Effect of filler surface activity and morphology on mechanical and dielectric properties of Nbr/Graphene nanocomposites *Rubber Chem. Technol.* **87** 70–85
[2] Chiricotto M, Giunta G, Karimi-Varzaneh H A and Carbone P 2020 Calculation of the work of adhesion of polyisoprene on graphite by molecular dynamics simulations *Soft Mater.* **18** 140–9
[3] Klüppel M 2003 The role of disorder in filler reinforcement of elastomers on various length scales *Adv. Polym. Sci.* **164** 1–86
[4] Hess W M and Klamp W K 1983 The effects of carbon black and other compounding variables on tire rolling resistance and traction *Rubber Chem. Technol.* **56** 390–417
[5] Pandey Y N, Brayton A, Burkhart C, Papakonstantopoulos G J and Doxastakis M 2014 Multiscale modeling of polyisoprene on graphite *J. Chem. Phys.* **140** 054908
[6] Mukherji D, Bartels G and Müser M H 2008 Scaling laws of single polymer dynamics near attractive surfaces *Phys. Rev. Lett.* **100** 068301
[7] De Virgiliis A, Milchev A, Rostiashvili V G and Vilgis T A 2012 Structure and dynamics of a polymer melt at an attractive surface *Eur. Phys. J.* E **35** 97
[8] Eslami H, Rahimi M and Müller-Plathe F 2013 Molecular dynamics simulation of a silica nanoparticle in oligomeric poly (methyl methacrylate): a model system for studying the interphase thickness in a polymer–nanocomposite via different properties *Macromolecules* **46** 8680–92
[9] Li J, Ding M, Zhang R and Shi T 2018 Effects of surface roughness on the self-diffusion dynamics of a single polymer *Soft Matter* **14** 3550–6
[10] Li J, Zhang R, Ding M and Shi T 2019 Unusual self-diffusion behaviors of polymer adsorbed on rough surfaces *J. Chem. Phys.* **150** 064902
[11] Carbone P and Avendaño C 2014 Coarse-grained methods for polymeric materials: enthalpy- and entropy-driven models *Wiley Interdiscip. Rev.-Comput. Mol. Sci.* **4** 62–70
[12] Raos G and Idé J 2014 Impact of interaction strength and surface heterogeneity on the dynamics of adsorbed polymers *ACS Macro Lett.* **3** 721–6
[13] Zheng Z, Li F, Liu J, Pastore R, Raos G, Wu Y and Zhang L 2018 Effects of chemically heterogeneous nanoparticles on polymer dynamics: insights from molecular dynamics simulations *Soft Matter* **14** 1219–26
[14] Pastore R, David A, Casalegno M, Greco F and Raos G 2019 Influence of wall heterogeneity on nanoscopically confined polymers *Phys. Chem. Chem. Phys.* **21** 772–9
[15] Schröder A, Klüppel M, Schuster R H and Heidberg J 2002 Surface energy distribution of carbon black measured by static gas adsorption *Carbon* **40** 207–10
[16] Giunta G, Svaneborg C, Karimi-Varzaneh H A and Carbone P 2020 Effects of graphite and plasticizers on the structure of highly entangled polyisoprene melts *ACS Appl. Polym. Mater.* **2** 317–25
[17] Donnet J B, Bansal R C and Wang M J 1993 *Carbon Black: Science and Technology* 2nd edn (Boca RatonTaylor & Francis) (https://doi.org/10.1201/9781315138763)
[18] Hall C E 1948 Dark-field electron microscopy: II. Studies of colloidal carbon *J. Appl. Phys.* **19** 271–7
[19] Everaers R, Karimi-Varzaneh H A, Fleck F, Hojdis N and Svaneborg C 2020 Kremer–Grest models for commodity polymer melts: linking theory, experiment, and simulation at the Kuhn scale *Macromolecules* **53** 1901–16
[20] Svaneborg C and Everaers R 2020 Characteristic time and length scales in melts of Kremer–Grest bead–spring polymers with wormlike bending stiffness *Macromolecules* **53** 1917–41
[21] Svaneborg C, Karimi-Varzaneh H A, Hojdis N, Fleck F and Everaers R 2016 Kremer–Grest models for universal properties of specific common polymer species (arXiv:1606.05008)
[22] Fetters L J, Lohse D J and Colby R H 2007 Chain dimensions and entanglement spacings *Physical Properties of Polymers Handbook* (New York: Springer)
[23] Grønbech-Jensen N, Hayre N R and Farago O 2014 Application of the G-JF discrete-time thermostat for fast and accurate molecular simulations *Comput. Phys. Commun.* **185** 524–7
[24] Abraham M J, Murtola T, Schulz R, Páll S, Smith J C, Hess B and Lindahl E 2015 GROMACS: high performance molecular simulations through multi-level parallelism from laptops to supercomputers *SoftwareX* **1-2** 19–25
[25] Hoeve C A J, DiMarzio E A and Peyser P 1965 Adsorption of polymer molecules at low surface coverage *J. Chem. Phys.* **42** 2558–63
[26] Acharya H, Vembanur S, Jamadagni S N and Garde S 2010 Mapping hydrophobicity at the nanoscale: applications to heterogeneous surfaces and proteins *Faraday Discuss.* **146** 353–65
[27] Heyes D M 2019 Translational and rotational diffusion of rod shaped molecules by molecular dynamics simulations *J. Chem. Phys.* **150** 184503
[28] Chung S H and Stevens J R 1991 Time-dependent correlation and the evaluation of the stretched exponential or Kohlrausch–Williams–Watts function *Am. J. Phys.* **59** 1024–30
[29] Li Y, Wei D, Han C C and Liao Q 2007 Dynamics of polymer melts confined by smooth walls: crossover from nonentangled region to entangled region *J. Chem. Phys.* **126** 204907
[30] Rissanou A N and Harmandaris V 2014 Dynamics of various polymer-graphene interfacial systems through atomistic molecular dynamics simulations *Soft Matter* **10** 2876–88
[31] Sharma P, Roy S and Karimi-Varzaneh H A 2019 Impact of plasticizer addition on molecular properties of polybutadiene rubber and its manifestations to glass transition temperature *Macromol. Theory Simul.* **28** 1900003
[32] Katsarou A F, Tsamopoulos A J, Tsalikis D G and Mavrantzas V G 2020 Dynamic heterogeneity in ring-linear polymer blends *Polymers* **12** 752
[33] Eslami H and Müller-Plathe F 2013 How thick is the interphase in an ultrathin polymer film? Coarse-grained molecular dynamics simulations of polyamide−6, 6 on graphene *J. Phys. Chem.* C **117** 5249–57
[34] Giunta G and Carbone P 2019 Cross-over in the dynamics of polymer confined between two liquids of different viscosity *Interface Focus* **9** 20180074